Spatial Distribution of Lipid Headgroups and Water Molecules at Membrane/Water Interfaces Visualized by Three-Dimensional Scanning Force Microscopy

Hitoshi Asakawa,[†] Shunsuke Yoshioka,[‡] Ken-ichi Nishimura,[‡] and Takeshi Fukuma[†,‡,*]
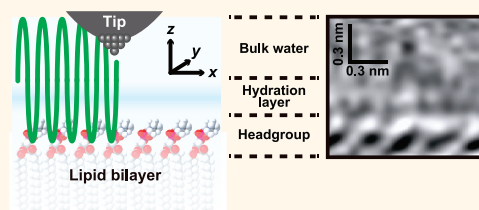
[†]Bio-AFM Frontier Research Center and [‡]Division of Electrical and Computer Engineering, Kanazawa University, Kanazawa, Japan

At the interface between a biological system and its surrounding physiological solution, water molecules interact with biomolecules constituting the surface. Through the interaction, water molecules have significant influence on the structure and function of biomolecules and their assembly.[1−3] Therefore, understanding the structure and function of a biological system requires investigations on the behavior of interfacial water. The surface of a biological membrane mainly consists of hydrophilic lipid headgroups. So far, the membrane/water interface has been extensively studied by various techniques.[4−11] These previous works have shown that the water molecules adjacent to a membrane strongly interact with the headgroups and have significant influence on its mechanical strength and fluidity.[12−14] However, the molecular-scale origin for such a critical influence has remained elusive.

One of the major difficulties in such a study lies in the measurement of molecular-scale structure of a membrane/water interface. As the lipid headgroups exhibit thermal fluctuations, the surface structure of a membrane is inherently ill-defined. In addition, the fluctuating lipid headgroups interact with mobile water, through which the interfacial water presents non-uniform density distribution known as hydration structure. Thus, the understanding of the whole structure of the membrane/water interface should require a method to visualize three-dimensional (3D) distribution of mobile water as well as fluctuating lipid headgroups.

Atomic force microscopy (AFM)[15] has been widely used as a nanoscale surface imaging tool. In a typical AFM setup, a sharp tip

ABSTRACT At biological interfaces, flexible surface structures and mobile water interact with each other to present non-uniform three-dimensional (3D) distributions. In spite of their impact on biological functions, molecular-scale understanding of such phenomena has remained elusive. Here we show direct visualization of such interfacial structures with subnanometer-scale resolution by 3D scanning force microscopy (3D-SFM). We measured a 3D force distribution at an interface between a model biological membrane and buffer solution by scanning a sharp tip within the 3D interfacial space. We found that vertical cross sections of the 3D image taken along a specific lateral direction show characteristic molecular-scale contrasts tilted at 30° to the membrane surface. Detailed analysis of the 3D image reveals that the tilted contrast corresponds to the time-averaged conformation of fluctuating lipid headgroups. On the basis of the obtained results, we discuss the relationships among the hydration structure, headgroup fluctuation, molecular fluidity, and mechanical strength of the membrane. The results demonstrate that 3D-SFM is capable of visualizing averaged 3D distribution of fluctuating surface structures as well as that of mobile water (*i.e.*, hydration structure) at interfaces between biological systems and water.

KEYWORDS: biological interface · lipid headgroup · 3D scanning force microscopy

is scanned in *XY* directions (*i.e.*, parallel to the surface) on a sample to produce a two-dimensional (2D) image of the surface topography. In contrast, several methods have recently been proposed for imaging 3D distribution of forces acting on a tip (F_t) near the sample surface.[16−21] In these methods, a tip is scanned in *Z* direction (*i.e.*, perpendicular to the surface) as well as in *XY* directions to image the whole 3D interfacial space. Among the proposed methods, 3D scanning force microscopy (3D-SFM)[20] has the fastest

imaging speed and hence is suitable for liquid environment applications where nonlinear tip drift is difficult to avoid.

Previously, 3D-SFM has been used for imaging 3D F_t distribution at a mica/water interface.[20] The obtained 3D image showed subnanometer-scale contrasts corresponding to the spatial distribution of a hydration layer and water molecules adsorbed on the surface. This previous work highlighted the unique capability of 3D-SFM to visualize hydration structures. However, the method has not been used for investigating a biological system. Thus, it has remained unknown how the fluctuating biomolecules and interfacial water are visualized and what information is obtained regarding their influence on the structure and functions of the biological system.

In this study, we investigate the membrane/water interface by 3D-SFM. We analyze subnanometer-scale contrasts of the measured 3D-SFM image and correlate them to the 3D distribution of interfacial water and fluctuating lipid headgroups. We also discuss the influence of hydration phenomena on the structure and dynamics of the lipid membrane.

RESULTS AND DISCUSSION

In this study, we have investigated a dipalmitoylphosphatidylcholine (DPPC) bilayer supported by mica. DPPC is one of the major phospholipids constituting a biological membrane. Thus, a DPPC bilayer has widely been used as a model biological membrane.[22−24] A DPPC has a tail group consisting of two acyl chains and a headgroup consisting of a zwitterionic phosphatidylcholine (PC) group (Figure 1a). In aqueous solution, DPPC molecules form a bilayer with the hydrophobic tail groups separated from water and the hydrophilic headgroups adjacent to water (Figure 1b). At room temperature, a DPPC bilayer is in the gel phase where the acyl chains are closely packed to exhibit relatively small thermal fluctuation. However, the headgroups
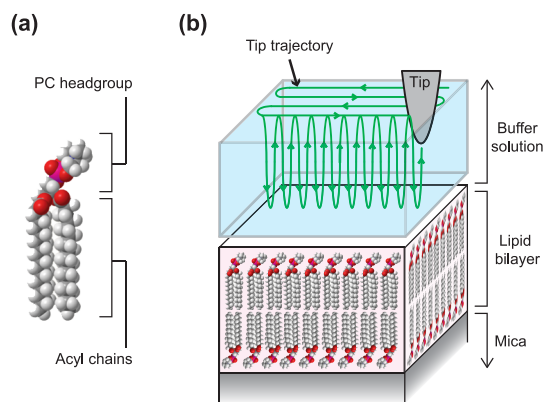

Figure 1. (a) Molecular structure of DPPC consisting of a phosphatidylcholine (PC) headgroup and acyl chains. (b) Illustration of 3D-SFM imaging at an interface between a DPPC bilayer and HEPES buffer solution. A tip is scanned in Z direction as well as in XY directions to image the whole 3D space at the interface.

exhibit much larger thermal fluctuation even in the gel phase due to the gap between adjacent headgroups.

We performed 3D-SFM imaging at the interface between the DPPC bilayer and HEPES solution. In 3D-SFM, the tip is laterally scanned on a sample as in the case of conventional AFM. During the scan, the vertical tip position (z_t) is modulated with a sine wave faster than the bandwidth of the tip−sample distance regulation (Figure 1b). The F_t values varied by the z_t modulation are recorded in real time to construct a 3D F_t image. In this experiment, z_t is modulated at 200 Hz with 1.73 $nm_{p−p}$ amplitude while the tip is laterally scanned at 12.2 nm/s. During the scan, the oscillation amplitude of the cantilever (A) was kept constant at 0.095 nm. The variation of F_t was detected as a shift (Δf) of the cantilever resonance frequency caused by F_t, namely, using frequency modulation (FM) detection method. In a single z_t modulation cycle, approaching and retracting Δf curves are obtained. In this study, we collected approaching Δf curves at each XY position to construct a 3D Δf image ($4 \times 4 \times 1.73$ nm³, $64 \times 64 \times 192$ pixels, 53 s per 3D image).

Figure 2a shows a model of the interface between the DPPC bilayer and water. The model consists of XY and Z cross sections extracted from the 3D Δf image. Figure 2b shows a Δf versus distance curve averaged over an XY cross section at each z_t. The Δf curve shows a gradual increase with oscillatory peaks. These features suggest the existence of a repulsive long-range force (F_{LR}) and an oscillatory short-range force (F_{SR}). We converted the Δf curve to F_t versus distance curve using the formula proposed by Sader and Jarvis.[25] The F_t curve (Figure 2c) shows that the oscillatory F_{SR} is much smaller than F_{LR}. However, the influence of F_{SR} is evident in the Δf curve. This is because FM-AFM has a high sensitivity to the force component with an interaction length comparable to A (0.095 nm in this experiment).[26]

In the previous study, Δf curves measured on a DPPC bilayer in phosphate buffered saline (PBS) solution showed an oscillatory profile without influence of F_{LR}.[11] This is due to the difference in the solution conditions used for the imaging and sample preparation. In fact, we experimentally confirmed the systematic difference between the Δf curves measured in HEPES and PBS solutions using different tips (see Supporting Information, Figure S1).

We estimated the F_{LR} component by fitting an exponential function to the F_t curve (dotted line in Figure 2c). We subtracted it from the original curve to obtain the F_{SR} component (Figure 2d). For the experiments in vacuum, F_{LR} originates from the electrostatic and van der Waals interactions. Thus, functions proportional to z_t^{-1} or z_t^{-2} are often used for the fitting.[27] In liquid, these force components are significantly suppressed, whereas the contribution of the hydration force becomes evident.[28] The distance dependence of the hydration force varies depending on the solution
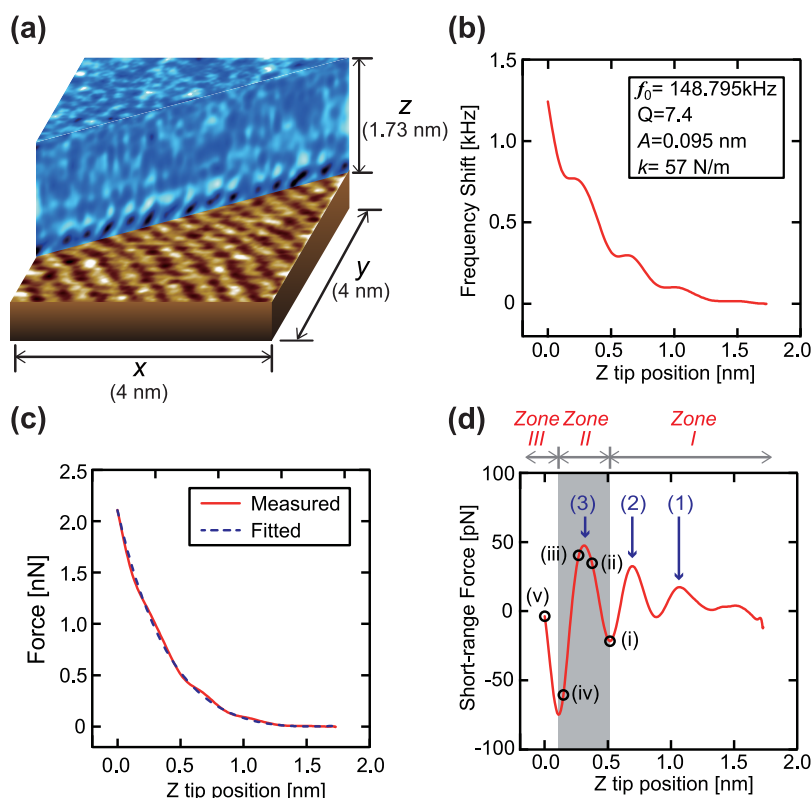
Figure 2. (a) Model of 3D-SFM image measured at the interface between the DPPC bilayer and HEPES buffer solution. (b) *XY*-averaged Δf versus z_t curve obtained from the 3D-SFM image. (c) Force *versus* z_t curve converted from the Δf curve shown in (b) (solid line) and the fitted curve (dotted line). (d) Short-range force (F_{SR}) *versus* z_t curve obtained by subtracting the fitted curve from the force curve shown in (c).

and tip conditions. It can be a monotonic increase, monotonic decrease, oscillation, or combination of them. Thus, it cannot be described by a simple formula. In this study, we used an exponential function as it is well-fitted to the measured F_t curve (Figure 2c). A similar method has been generally used for analyzing the force curves measured by surface force apparatus (SFA).[29]

The F_{SR} curve shows an oscillatory profile with three peaks (1) to (3) (Figure 2d). The peak separation between peaks (1) and (2) is $D_{12} = 0.36$ nm, while that between peaks (2) and (3) is $D_{23} = 0.38$ nm. Such an oscillatory profile has also been observed in the force curves obtained in the previous studies using AFM[30] or SFA.[31] Due to the agreement between the measured peak separation and the expected thickness of a water layer (0.2−0.4 nm), the oscillatory profile has been considered to reflect the layered distribution of the interfacial water (*i.e.*, hydration layers). In fact, force curves measured at a mica/water interface in the previous study using FM-AFM[20] showed good agreement with the results obtained by Monte Carlo simulation[32] and X-ray reflectometry,[33] which supports the above discussion.

In contrast to the mica surface, the membrane surface consists of flexible lipid headgroups. Thus, oscillatory force peaks may arise when the tip penetrates into the headgroup region. This means that we cannot identify the position of the hydration layers or headgroup

region from the averaged force curve. However, we have the whole data of the 3D force distribution so that we should be able to obtain additional information to answer this question by analyzing *XY* cross sections of the 3D Δf image as shown below.

For detailed analysis of F_{SR}, we obtained a 3D F_{SR} image by applying the same procedure as shown in Figure 2b−d to all of the Δf curves constituting the 3D-SFM image. Movie 1 in Supporting Information shows *XY* cross sections of the 3D F_{SR} image at different z_t positions. Figure 3 shows selected *XY* cross sections obtained at z_t positions (i) to (v) indicated in Figure 2d. Here we explain the z_t dependence of the *XY* cross section using Figure 2d and Figure 3. The *XY* cross section shows no specific contrasts above position (i) (zone I) as shown in Figure 3a. With decreasing z_t from position (i), the *XY* cross section gradually starts to show molecular-scale contrast. This contrast marks the highest clarity at position (ii), which is slightly higher than the position of peak (3), as shown in Figure 3b. However, as z_t is decreased from the position of peak (3), the bright spots corresponding to the individual molecules become unclear and appear to be connected to form a striped contrast (Figure 3c). With further decrease of z_t, the molecular-scale contrast appears only in a narrow z_t range around position (iv) (Figure 3d). However, this contrast is not as clear as that
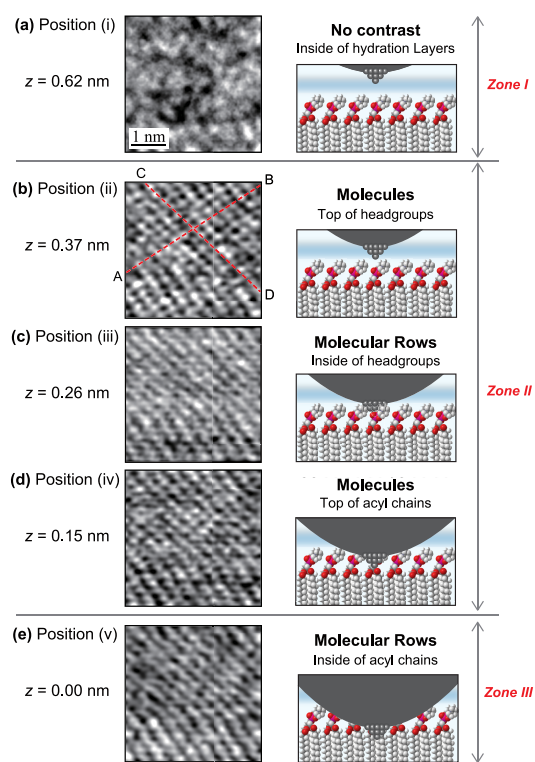
Figure 3. XY cross sections obtained from the 3D F_{SR} image of the interface between the DPPC bilayer and HEPES buffer solution. Positions (i) to (v) are indicated in Figure 2d. Illustrations show the relative positions of the tip apex with respect to the membrane surface. (b−e) Orientation of the molecular rows appears to be slightly changed at the middle of the image. This is due to nonlinear drift of the tip position with respect to the sample surface.

observed at position (ii) (Figure 3b). Below position (iv) (zone III), only the striped features corresponding to the molecular rows are observed (Figure 3e). In addition, the distortion of the striped contrasts increases with decreasing z_t.

The results show that the molecular-scale contrasts are observed only in the z_t range from position (i) to (iv) (zone II). From the operation principle of AFM, a molecular-resolution image with the highest resolution and lowest distortion (Figure 3b at position (ii)) should be obtained when the tip is scanned on top of the headgroups. Thus, the position of peak (3) should correspond to the headgroup region. In fact, this interpretation allows us to consistently explain all of the experimental results. For example, the lack of molecular-scale contrasts above position (i) is explained by the existence of mobile water in zone I. The gradual enhancement of the molecular-scale contrast from position (i) to (ii) is explained by the gradual increase of the interaction between the tip and headgroups. The increase of the image distortion from position (ii) to (iii) is explained by the penetration of the tip into the headgroup region. The reappearance of the molecular-scale contrast near position (iv) is explained by an increase of the interaction between

the tip and the top of the stable acyl chains. The increase of the image distortion from position (iv) to (v) is explained by the tip penetration into the acyl chain region. All of these results support the above interpretation.

Conversely, other interpretations do not allow us to explain all of the experimental results. For example, if the headgroups are at the position of peak (1) or (2), molecular-scale contrasts should be observed around these peaks. If the headgroups are below the position of peak (3), the molecular-scale contrasts observed at position (ii) should be much weaker than that observed between positions (iv) and (v) due to the existence of a water layer between the tip and headgroups. Therefore, these two assumptions contradict the experimental results.

From these analyses, we have concluded that the headgroups are at the position of peak (3). Accordingly, zones I−III should correspond to the positions of the hydration layers, lipid headgroups, and acyl chains, respectively.

To investigate lateral distribution of the headgroups and hydration layers in zones I and II, we have obtained Z cross sections of the 3D F_{SR} image (Figure 4). Figure 4a,b shows the Z cross sections obtained along lines A-B and C-D in Figure 3b, respectively. Figure 4c shows the same F_{SR} curve as shown in Figure 2d but with the z_t scale matched to the vertical scale of the Z cross sections. In zone I, the both Z cross sections show uniform and layered contrasts corresponding to the bulk water and first hydration layer, respectively. Thus, no significant difference is observed. In contrast, the Z cross sections show clear difference in zone II. Namely, a molecular-scale contrast consisting of stripes tilted to the Z axis is observed only in Figure 4a, and such a contrast is not observed in Figure 4b. We also examined other Z cross sections and confirmed that such a contrast is observed only in the cross sections taken along a molecular row nearly parallel to line A-B (see Supporting Information, movies 2 and 3). The result suggests that the interaction force acting between the tip and headgroups has rotational anisotropy with respect to the Z axis.

The tilted contrasts are observed only in zone II, where interaction between the tip and the headgroups predominantly contributes to the contrast formation. Thus, the observed contrast should reflect the rotational anisotropy of the tip or the headgroups. For this particular experiment, the latter is more likely to be the case as discussed below. According to the previous studies using molecular dynamics (MD) simulation, the DPPC headgroups exhibit thermal fluctuations even in the gel phase at room temperature. However, the fluctuation is not random but has preference. On average, the headgroups are oriented to a specific direction and tilted at 30° to the membrane surface.[22,34−36] The fluctuation of the headgroups is much
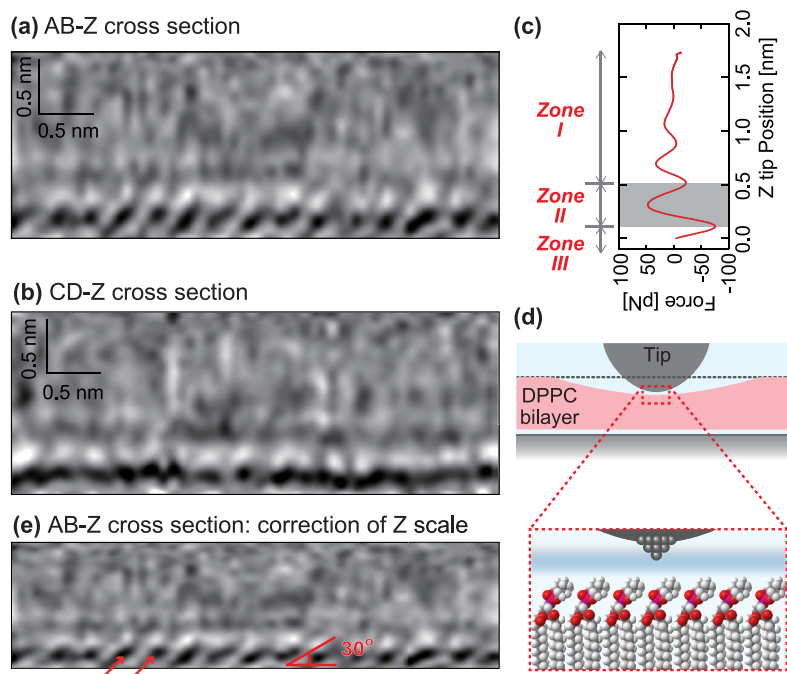
(a) AB-Z cross section

0.5 nm

0.5 nm

(b) CD-Z cross section

0.5 nm

0.5 nm

(e) AB-Z cross section: correction of Z scale

30°

(c)

Zone I

Zone II

Zone III

Z tip Position [nm]

Force [pN]

(d)

Tip

DPPC bilayer

Figure 4. Z cross sections of the 3D F_{SR} image obtained along lines A-B (a) and C-D (b) in Figure 3b. (c) Same F_{SR} curve as shown in Figure 2d with the z_t scale matched to the vertical scale of (a) and (b). (d) Schematic illustration showing the deformation of the DPPC bilayer caused by F_{LR}. (e) Corrected AB-Z cross section.

faster than the imaging speed of 3D-SFM. Thus, the measured force should reflect the time-averaged interaction between the quasi-static tip and the headgroups with their position and orientation thermally fluctuated. When the tip is placed at the averaged position of a headgroup, the headgroup is hindered to take the favorable conformation during the fluctuation. Consequently, a large repulsive force should be applied to the tip apex. Therefore, the force distribution measured by 3D-SFM should reflect the time-averaged structure of the DPPC headgroups.

The striped contrasts in Figure 4a are tilted at 55° to the membrane surface, which is larger than the tilt angle of a PC headgroup expected from the MD simulation (≈30°). Although this result seems to contradict the above argument, it can be consistently explained by taking into account the deformation of the DPPC bilayer caused by F_{LR}. The F_{SR} acting between each headgroup and the atomic-scale tip apex is lower than 100 pN, as shown in Figure 2d. However, the F_{LR} acting on all of the DPPC molecules contained in the nanoscale interaction range becomes higher than 1 nN when the tip is brought into contact with the headgroups (Figure 2c). If the bilayer is deformed by the F_{LR}, as shown in Figure 4d, it can lead to an error in the measured tilt angle of the headgroups.

Here we estimate the deformation of the bilayer caused by F_{LR}. We assume that the bilayer shows elastic deformation in proportion to the F_{LR} curve obtained by the fitting shown in Figure 2c. We have confirmed the validity of this assumption by taking force curves

($n = 88$) by static-mode AFM on a DPPC bilayer prepared under the same conditions as used in the 3D-SFM experiment. Figure 5a shows a typical force curve measured on the DPPC bilayer in HEPES buffer solution. The curve shows a jump (as indicated by an arrow in Figure 5a) corresponding to the penetration of the AFM tip into the DPPC bilayer. The linear force increase before the penetration suggests that the DPPC bilayer shows elastic deformation by the interaction with the nanoscale AFM tip. Thus, the stiffness of the DPPC bilayer (k_{LB}) can be calculated with a series spring model shown in Figure 5b. The effective stiffness of the series spring (k_{EF}) was estimated from the slope of the force curve as shown in Figure 5a. From k_{EF} and k_{CL}, k_{LB} was calculated by $k_{LB} = k_{EF}k_{CL}/(k_{CL} - k_{EF})$. We calculated k_{CL} with individual force curves and obtained their average of 12 ± 2.7 N/m (Figure 5c).

Similar to the case in the static-mode AFM measurement, we should take into account the static bending of the cantilever caused by F_{LR} in the 3D-SFM measurement. For this purpose, we can use the same series spring model as shown in Figure 5b. From the estimated k_{LB} and the equation $k_{EF} = k_{CL}k_{LB}/(k_{CL} + k_{LB})$, we obtained k_{EF} of 8.5 N/m. From the k_{EF} and the F_{LR} curve (Figure 2c), we obtained a deformation *versus* distance curve and used it for correcting the z_t scale of the Z cross section shown in Figure 4a. The corrected Z cross section is shown in Figure 4e.

Comparing Figure 4a and 4e, we find little difference in zone I corresponding to the water region. For example, the distance between peaks (1) and (2) is
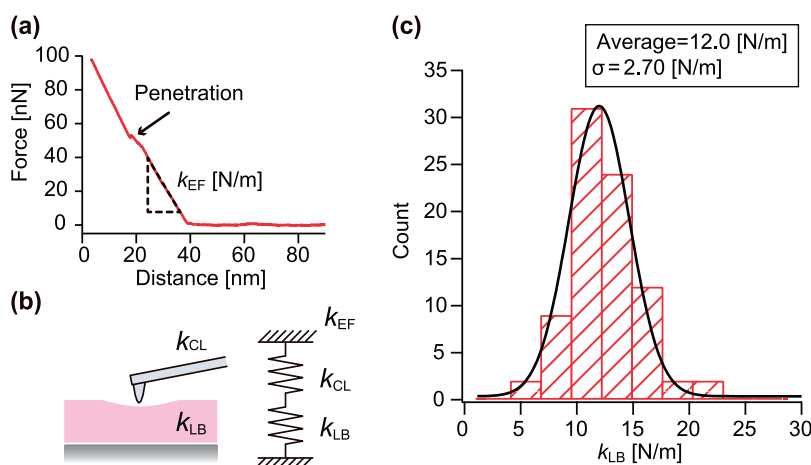
Figure 5. Force curve measurements by static-mode AFM for the investigation of the effective stiffness of the DPPC bilayer (k_{LB}). (a) Typical force curve measured on the DPPC bilayer. (b) Series spring model. (c) Histogram of the k_{LB} values estimated from the force curves and the series spring model.

decreased only by 0.02 nm from 0.36 to 0.34 nm. In contrast, the force distribution in zone II corresponding to the headgroup region is significantly compressed in Z direction. This is because F_{LR} increases with decreasing z_t, and hence, the influence of the z_t scale correction becomes prominent near the membrane surface. In the corrected Z cross section (Figure 4e), the tilt angle of the striped contrast ($\approx 30°$) agrees with the value expected from the MD simulation. The result supports our argument that the tilted contrasts reflect the averaged conformation of the fluctuating headgroups.

As explained above, the tip feels strong repulsive force when it is placed at the averaged position of the fluctuating headgroup. Thus, the averaged conformation is imaged with a bright contrast. However, the decrease of F_{SR} below the headgroup position (arrows in Figure 4e) should require additional explanation. As the tip approaches the averaged position of a headgroup, the repulsive force gradually increases. When the force exceeds a threshold value, the most favorable conformation of the headgroup should be changed. Thus, the averaged headgroup position is displaced from under the tip, and the repulsive force is decreased. This explains the imaging mechanism of the tilted contrast corresponding to the headgroup conformation (Figure 4e). Although the contrast may not perfectly represent the true headgroup structure, the orientation and tilted angle are likely to agree with those of the averaged headgroup conformation.

Here, we discuss possibilities of the other origins of the tilted contrast. One possible origin is the deformation of the tip apex. In fact, tilted contrasts can be observed even at a mica/water interface when we use a large loading force to deform the tip apex. In our experiment, however, the tip interacts with fluctuating headgroups. Thus, the averaged headgroup conformation is likely to be changed before the Si tip is deformed. Another possible origin is the deformation of acyl chains. For example, contact-mode AFM images

of lipid bilayers show distorted molecular-scale contrasts due to the molecular deformation when a large loading force is used.[37] In our experiment, however, we experimentally confirmed that the tilted contrast does not change when the fast scanning direction is inverted. Thus, the tilted contrast is unlikely to be caused by the lateral loading force. We also estimated the vertical deformation caused by F_{LR} from k_{LB} and Figure 2c. At z_t range of 0.0–0.3 nm, the vertical deformation is ≈ 0.1 nm. However, the lateral shift of the tilted contrast is about ≈ 0.35 nm, which is much larger than the vertical deformation. Therefore, it is unlikely that the tilted contrast is caused by the vertical loading force either. From these discussions, it is most likely that the tilted contrast reflects the averaged conformation of the fluctuating headgroups.

The distance between peaks (1) and (2) (*i.e.*, the first and second hydration layers) is 0.34 nm in the corrected Z cross section (Figure 4e). This is longer than the value previously measured in PBS solution (0.28 nm).[11] We performed separate experiments to compare the properties of a DPPC bilayer in HEPES and PBS solution. We found that a DPPC bilayer in HEPES solution shows longer repulsive F_{LR} (see Supporting Information, Figure S1) and lower mechanical strength (see Supporting Information, Table S1) than that in PBS solution. The lower mechanical strength suggests larger molecular fluidity and fluctuation of the molecules, which has been considered to be an origin of repulsive F_{LR}.[28] Therefore, these results suggest the larger fluctuation of the DPPC molecules in HEPES solution and its influence on the hydration force. Similarly, the molecular fluctuation may disturb the layer-like distribution of the water molecules, leading to the larger spacing between the hydration layers. In fact, the distance between the hydration layers measured on inorganic crystals having low fluctuation is typically smaller than that on DPPC bilayers. For example, it has been reported to be 0.27 nm on mica,[19] 0.20 nm on
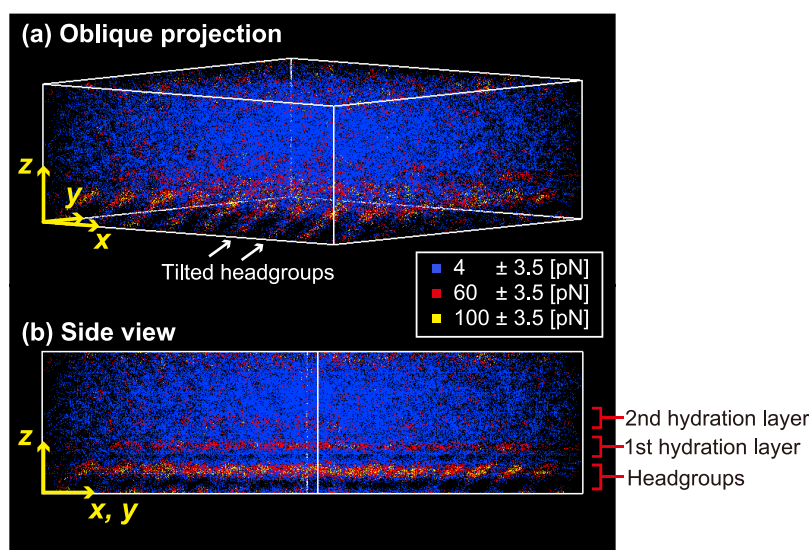
Figure 6. Scatter plot of the 3D F_{SR} image. (a) Oblique projection. (b) Side view.

calcite,[30] and 0.22 nm on self-assembled monolayer of COOH(CH$_2$)$_{10}$—SH/Au(111).[38] These results support the above argument that the surface fluctuation may influence the distance of hydration layers. Future experiments with different lipid headgroups and ionic species may elucidate detailed correlation between the fluctuation of surface molecules and the 3D hydration structure.

CONCLUSION

In this study, we measured 3D force distribution at the interface between fluctuating lipid headgroups and HEPES buffer solution. The obtained 3D image shows molecular-scale tilted contrasts reflecting the averaged conformation of the headgroups as well as layer-like contrasts corresponding to the hydration layer (Figure 6). The results demonstrate that we can visualize averaged 3D distribution of fluctuating surface structures as well as that of mobile water (i.e., hydration structure). We performed detailed analysis of the 3D image and discussed the relationships among the hydration structure, headgroup fluctuation, molecular fluidity, and mechanical strength of the membrane. There are many other examples where local interaction between fluctuating structures and water influences structure and dynamics of biological systems. However, the information obtained by the conventional techniques is not necessarily sufficient to achieve molecular-scale understanding of such interfacial phenomena. The results obtained in this study suggest that 3D-SFM can complement the missing piece of information. This unique capability should contribute to the progress in the molecular-scale understanding of the various phenomena at biological interfaces.

EXPERIMENTAL SECTION

Preparation of DPPC Bilayer. DPPC molecules in powder form (Avanti Polar Lipids, Inc.) were dissolved in a mixture of chloroform and methanol (3:1, v/v) to a concentration of 1 mg/mL. The DPPC solution in a glass test tube was dried in N$_2$ gas flow to form a lipid thin film at the bottom of the tube. The 4-(2-hydroxyethyl)-1-piperazineethanesulfonic acid (HEPES) buffer solution (10 mM HEPES, 100 mM sodium chloride, pH 7.4) with Ca^{2+} (3 mM CaCl$_2$) was poured into the test tube to the final concentration of 0.5 mg/mL. The test tube was incubated at 60 °C for 1 h to hydrate and disperse the lipid film. The solution was passed through a Nucleopore polycarbonate membrane with 100 nm mean pore diameter (Mini-extruder system, Avanti Polar Lipids, Inc.), yielding a solution of unilamellar vesicles of uniform size. Then, 240 μL of the solution was deposited to a cleaved mica substrate with a diameter of 12 mm (SPI Supplies). The sample was incubated at 60 °C for 1 h and rinsed with the HEPES buffer solution after cooling to a room temperature. All of the AFM experiments were performed at room temperature (22 °C), which is below the main phase transition temperature (T_m) of a DPPC bilayer. The obtained DPPC bilayer has some local defects. The step height measured at the defect edge corresponds to the typical thickness of a DPPC bilayer (≈4.5 nm), which confirmed the formation of a single bilayer on mica (see Supporting Information, Figure S2).

AFM Measurements. A custom-built FM-AFM with a low noise cantilever deflection sensor[39−41] was used for the 3D-SFM imaging. A commercially available AFM controller (ARC2, Asylum Research) was used for controlling the FM-AFM with modifications in the software. We used a silicon cantilever (PPP-NCH, Nanoworld) having a resonance frequency (f_0) of 148.795 kHz, a spring constant (k_{CL}) of 57 N/m, and Q factor of 7.4 in the HEPES buffer solution. For the measurements of the force curves by static-mode AFM, we used a relatively soft cantilever (k_{CL} = 3.15 N/m, PPP-FM, Nanoworld).

Conflict of Interest: The authors declare no competing financial interest.

Supporting Information Available: Additional figures, a table, and movies. This material is available free of charge via the Internet at http://pubs.acs.org.

REFERENCES AND NOTES

1. Ge, M.; Freed, J. H. Hydration, Structure and Molecular Interactions in the Headgroup Region of Dioleoylphosphatidylcholine Bilayers: An Electron Spin Resonance Study. *Biophys. J.* **2003**, *85*, 4023–4040.

2. Ball, P. Water as an Active Constituent in Cell Biology. *Chem. Rev.* **2008**, *108*, 74–108.

3. Levy, Y.; Onuchic, J. N. Water Mediation in Protein Folding and Molecular Recognition. *Annu. Rev. Biophys. Biomol. Struct.* **2006**, *35*, 389–415.

4. Nagle, J. F.; Tristram-Nagle, S. Structure of Lipid Bilayers. *Biochim. Biophys. Acta* **2000**, *1469*, 159–195.

5. Milhaud, J. New Insights into Water-Phospholipid Model Membrane Interactions. *Biochim. Biophys. Acta* **2004**, *1663*, 19–51.

6. Márazková, E.; Hobza, P.; Bohl, M.; Gauger, D. R.; Pohle, W. Hydration-Induced Changes of Structure and Vibrational Frequencies of Methylphosphocholine Studied as a Model of Biomembrane Lipids. *J. Phys. Chem. B* **2005**, *109*, 15126–15134.

7. Sýkora, J.; Kapusta, P.; Fidler, V.; Hof, M. On Water Time Scale Does Solvent Relaxation in Phospholipid Bilayers Happen? *Langmuir* **2002**, *18*, 571–574.

8. Berkowitz, M. L.; Bostick, D. L.; Pandit, S. Aqueous Solutions Next to Phospholipid Membrane Surfaces: Insights from Simulations. *Chem. Rev.* **2006**, *106*, 1527–1539.

9. Cheng, J.; Pautot, S.; Weitz, D. A.; Xie, X. S. Ordering of Water Molecules between Phospholipid Bilayers Visualized by Coherent Anti-Stokes Raman Scattering Microscopy. *Proc. Natl. Acad. Sci. U.S.A.* **2003**, *100*, 9826–9830.

10. Higgins, M.; Polcik, M.; Fukuma, T.; Sader, J.; Nakayama, Y.; Jarvis, S. P. Structured Water Layers Adjacent to Biological Membranes. *Biophys. J.* **2006**, *91*, 2532–2542.

11. Fukuma, T.; Higgins, M. J.; Jarvis, S. P. Direct Imaging of Individual Intrinsic Hydration Layers on Lipid Bilayers at Angstrom Resolution. *Biophys. J.* **2007**, *92*, 3603–3609.

12. Pasenkiewicz-Gierula, M.; Takaoka, Y.; Miyagawa, H.; Kitamura, K.; Kusumi, A. Hydrogen Bonding of Water to Phosphatidylcholine in the Membrane as Studied by a Molecular Dynamics Simulation: Location, Geometry, and Lipid—Lipid Bridging *via* Hydrogen-Bonded Water. *J. Phys. Chem. A* **1997**, *101*, 3677–3691.

13. Fitter, J.; Lechner, R. E.; Dencher, N. A. Interactions of Hydration Water and Biological Membranes Studied by Neutron Scattering. *J. Phys. Chem. B* **1999**, *103*, 8036–8050.

14. Zhao, W.; Moilanen, D. E.; Fenn, E. E.; Fayer, M. D. Water at the Surface of Aligned Phospholipid Multibilayer Model Membranes Probed with Ultrafast Vibrational Spectroscopy. *Biophys. J.* **2008**, *130*, 13927–13937.

15. Binnig, G.; Quate, C. F.; Gerber, C. Atomic Force Microscope. *Phys. Rev. Lett.* **1986**, *56*, 930–933.

16. Hölscher, H.; Langkat, S. M.; Schwarz, A.; Wiesendanger, R. Measurement of Three-Dimensional Force Fields with Atomic Resolution Using Dynamic Force Spectroscopy. *Appl. Phys. Lett.* **2002**, *81*, 4428–4430.

17. Albers, B. J.; Schwendemann, T. C.; Baykara, M. Z.; Pilet, N.; Liebmann, M.; Altman, E. I.; Schwarz, U. D. Three-Dimensional Imaging of Short-Range Chemical Forces with Picometre Resolution. *Nat. Nanotechnol.* **2009**, *4*, 307–310.

18. Ternes, M.; Lutz, C. P.; Hirjibehedin, C. F.; Giessibl, F. J.; Heinrich, A. J. The Force Needed To Move an Atom on a Surface. *Science* **2008**, *1319*, 1066–1069.

19. Kimura, K.; Ido, S.; Oyabu, N.; Kobayashi, K.; Hirata, Y.; Imai, T.; Yamada, H. Visualizing Water Molecule Distribution by Atomic Force Microscopy. *J. Chem. Phys.* **2010**, *132*, 194705–194709.

20. Fukuma, T.; Ueda, Y.; Yoshioka, S.; Asakawa, H. Atomic-Scale Distribution of Water Molecules at the Mica—Water Interface Visualized by Three-Dimensional Scanning Force Microscopy. *Phys. Rev. Lett.* **2010**, *104*, 016101–016104.

21. Welker, J.; Giessibl, F. J. Revealing the Angular Symmetry of Chemical Bonds by Atomic Force Microscopy. *Science* **2012**, *336*, 444–449.

22. Tu, K.; Tobias, D. J.; Blasie, J. K.; Klein, M. L. Molecular Dynamics Investigation of the Structure of a Fully Hydrated Gel-Phase Dipalmitoylphosphatidylcholine Bilayer. *Biophys. J.* **1996**, *70*, 595–608.

23. Tu, K.; Klein, M. L.; Tobias, D. J. Constant-Pressure Molecular Dynamics Investigation of Cholesterol Effects in a Dipalmitoylphosphatidylcholine Bilayer. *Biophys. J.* **1998**, *75*, 2147–2156.

24. Xu, X.; London, E. The Effect of Sterol Structure on Membrane Lipid Domain Reveals How Cholesterol Can Induce Lipid Domain Formation. *Biochemistry* **2000**, *39*, 843–849.

25. Sader, J. E.; Jarvis, S. P. Accurate Formulas for Interaction Force and Energy in Frequency Modulation Force Spectroscopy. *Appl. Phys. Lett.* **2004**, *84*, 1801–1803.

26. Giessibl, F. J.; Bielefeldt, H.; Hembacher, S.; Mannhart, J. Calculation of the Optimal Imaging Parameters for Frequency Modulation Atomic Force Microscopy. *Appl. Surf. Sci.* **1999**, *140*, 352–357.

27. Langkat, S. M.; Hölscher, H.; Schwarz, A.; Wiesendanger, R. Determination of Site Specific Interatomic Forces between an Iron Coated Tip and the NiO(001) Surface by Force Field Spectroscopy. *Surf. Sci.* **2003**, *527*, 12–20.

28. Israelachvili, J. N. *Intermolecular and Surface Forces*, 3rd ed.; Elsevier: Amsterdam, 2011; pp 341−380

29. Chapel, J. P. Electrolyte Species Dependent Hydration Forces between Silica Surfaces. *Langmuir* **1994**, *10*, 4237–4243.

30. Cleveland, J. P.; Schäffer, T. E.; Hansma, P. K. Probing Oscillatory Hydration Potentials Using Thermal-Mechanical Noise in an Atomic-Force Microscope. *Phys. Rev. B* **1995**, *52*, 8692–8695.

31. Israelachvili, J. N.; Pashley, R. M. Molecular Layering of Water at Surfaces and Origin of Repulsive Hydration Forces. *Nature* **1983**, *306*, 249–250.

32. Park, S. H.; Sposito, G. Structure of Water Adsorbed on a Mica Surface. *Phys. Rev. Lett.* **2002**, *89*, 085501–085503.

33. Cheng, L.; Fenter, P.; Nagy, K. L.; Schlegel, M. L.; Sturchio, N. C. Molecular-Scale Density Oscillations in Water Adjacent to a Mica Surface. *Phys. Rev. Lett.* **2001**, *87*, 156103–156106.

34. Pink, D. A.; Belaya, M.; Levadny, V.; Quinn, B. A Model of Polar Group Statics in Lipid Bilayers and Monolayers. *Langmuir* **1997**, *13*, 1701–1711.

35. Lópes-Cascales, J.; Otero, T. F.; Fernández-Romero, L.; Camachoe, A. J. Phase Transition of a DPPC Bilayer Induced by an External Surface Pressure: From Bilayer to Monolayer Behavior. A Moleculer Dynamics Simulation Study. *Langmuir* **2006**, *22*, 5818–5824.

36. Mbamala, E. C.; Fahr, A.; May, S. Electrostatic Model for Mixed Cationic-Zwitterionic Lipid Bilayers. *Langmuir* **2006**, *22*, 5129–5136.

37. Beckmann, M.; Nollert, P.; Kolb, H.-A. Manipulation and Molecular Resolution of a Phosphatidylcholine-Supported Plannar Bilayer by Atomic Force Microscopy. *J. Membr. Biol.* **1998**, *161*, 227–233.

38. Jarvis, S. P.; Uchihashi, T.; Ishida, T.; Tokumoto, H.; Nakayama, Y. Local Solvation Shell Measurement in Water Using Carbon Nanotube Probe. *J. Phys. Chem. B* **2000**, *104*, 6091–6094.

39. Fukuma, T.; Kimura, M.; Kobayashi, K.; Matsushige, K.; Yamada, H. Development of Low Noise Cantilever Deflection Sensor for Multienvironment Frequency-Modulation Atomic Force Microscopy. *Rev. Sci. Instrum.* **2005**, *76*, 053704–053711.

40. Fukuma, T.; Jarvis, S. P. Development of Liquid-Environment Frequency Modulation Atomic Force Microscope with Low Noise Deflection Sensor for Cantilevers of Various Dimensions. *Rev. Sci. Instrum.* **2006**, *77*, 043701–043708.

41. Fukuma, T. Wideband Low-Noise Optical Beam Deflection Sensor with Photothermal Excitation for Liquid-Environment Atomic Force Microscopy. *Rev. Sci. Instrum.* **2009**, *80*, 023707–023714.